Novel Synthesis and Thermal Behavior of Aluminum Hydroxy Fluorides $AlF_x(OH)_{3-x}$

Christoph Stosiek,[†] Gudrun Scholz,[†] Gehan Eltanany,[†] Rainer Bertram,[‡] and Erhard Kemnitz*,[†]

Institut für Chemie, Humboldt Universität zu Berlin, Brook Taylor Strasse 2, Berlin, 12489 Germany, and Institut für Kristallzüchtun, Max Born-Strasse 2, Berlin, 12489 Germany

Received May 6, 2008. Revised Manuscript Received July 3, 2008

A new synthesis route to nonhydrated, X-ray amorphous aluminum hydroxy fluorides was explored by sol−gel synthesis with aqueous hydrofluoric acid. Followed by XRD, MAS NMR, and DTA-TG, it can be shown that the product composition after thermal annealing critically depends on the gaseous atmosphere. Dependent on the fluorine content, corundum formation can occur at temperatures as low as 900 °C. Additional mechanical activation of the starting material enhances effects of pyrohydrolysis on thermal annealing and consequently favors early corundum formation in addition.

1. Introduction

In the past few decades, the improvement of the properties of ceramic materials has been of great interest. In the field of engineering ceramics and especially for aluminum oxide ceramics, the requirements of purity and easy accessibility of the raw material (e.g., gibbsite or pseudoboehmite) were important. Because of economical reasons, there is a large interest in lowering the temperature of phase transition of the raw material to corundum. In addition, product properties are strongly affected by annealing temperature. Therefore, thermal annealing of gibbsite (γ-$Al(OH)_3$) or pseudoboehmite (AlOOH-xerogel) at high temperatures leads to an abnormal grain growth and a reduced density after sintering.[1−3]

By using thermoanalytical methods, several studies into the reduction of the temperature of phase transition for the raw powder material ($Al(OH)_3$, AlOOH) to corundum took place: Kano et al. reduced the transition temperature to 910 °C by high-energy ball milling.[3] Nofz et al. investigated the influence of corundum seeding and iron doping on the phase transition temperature of pseudoboehmite. They found a decrease in the temperature of corundum formation of about 150 °C−200 °C, dependent on the pretreatment of the samples.[4,5] Cava et al. determined the phase transformation of cobalt doped γ-Al_2O_3 and found a temperature decrease of about 150 °C.[6] The doping of the raw materials with lanthanum obviously has an opposite effect. Loong et al. found an increase in temperature of phase transition from γ-Al_2O_3 to α-Al_2O_3 of about 120 °C.[7]

Fluorides have a great influence on the transition temperature to corundum. Zivkovic et al. investigated the effect of fluoride doping of γ-Al_2O_3 (AlF_3, CaF_2, MgF_2, LiF, NaF, and Na_3AlF_6) on the corundum formation.[8] They have shown that doping with AlF_3 leads to the greatest effect (phase transition at 900 °C) followed by MgF_2 (1080 °C) and CaF_2 (1170 °C). Li et al.[9] and Wu et al.[10] achieved similar results with mixtures of pseudoboehmite and AlF_3 or ZnF_2, respectively, but unlike Zivkovic et al.,[8] they also obtained a decrease in the phase transition temperature comparable with AlF_3 by the use of LiF.

In most cases, the use of such additives leads to a contamination of the final corundum powder with chemical impurities that can cause undesired characteristics of the sintering product.[11] In the case of aluminum fluoride as additive the impurities are mainly limited to fluoride. By using of $AlF_x(OH)_{3-x}$ as precursor compounds without additional doping, partial dehydroxylation at low temperature can take place and afterward hydrolysis of the oxide fluoride at higher temperatures (pyrohydrolysis). The combination of both effects could result in a complete removal of the fluoride content and might cause an early corundum formation.

Therefore, the aims of the present study are

(i) to prepare nanoscaled aluminum hydroxy fluorides and aluminum fluorides with varying Al/F ratio by sol−gel synthesis

(ii) to investigate the influence of different gas atmospheres on the product formation at thermal annealing, and

(iii) to obtain oxidic phases without chemical impurities by annealing the aluminum hydroxy fluorides.

* Corresponding author. Fax: 49 (0)30 2093 7277. E-mail: erhard.kemnitz@chemie.hu-berlin.de.

[†] Humboldt Universität zu Berlin.

[‡] Institut für Kristallzüchtun.

(1) Bae, S. I.; Baik, S. *J. Am. Ceram. Soc.* **1993**, *76*, 1065.
(2) Bae, I.-J.; Baik, S. *J. Am. Ceram. Soc.* **1997**, *80*, 1149.
(3) Kano, J.; Saeki, S.; Saito, F.; Saeki, S.; Tanjo, M.; Yamazaki, S. *Int. J. Miner. Process* **2000**, *60*, 91.
(4) Nofz, M.; Stösser, R.; Scholz, G.; Dörfel, I.; Schultze, D. *J. Eur. Ceram. Soc.* **2005**, *25*, 1095.
(5) Stöβer, R.; Nofz, M.; Feist, M.; Scholz, G. *J. Solid State Chem.* **2006**, *179*, 652.
(6) Cava, S.; Tebcherani, S. M.; Pianaro, S. A.; Paskocimas, C. A.; Longo, E.; Varela, J. A. *Mater. Chem. Phys.* **2006**, *97*, 102.
(7) Loong, C. K.; Richardson, J. W., Jr.; Ozawa, M. *J. Alloys Compd.* **1997**, *250*, 356.
(8) Zivkovic, Z.; Strbac, N.; Sestak, J. *Thermochim. Acta* **1995**, *266*, 293.
(9) Li, J.; Wu, Y.; Pan, Y.; Liu, W.; Guo, J. *Ceram. Int.* **2007**, *33*, 919.
(10) Wu, Y.; Zhang, Y.; Pezzotti, G.; Guo, J. *Mater. Lett.* **2002**, *52*, 366.
(11) Sathiyakumar, M.; Gnanam, F. D. *Ceram. Int.* **2002**, *28*, 195.

10.1021/cm801236v CCC: $40.75
Published on Web 08/15/2008

Aluminum hydroxy fluorides can be formed in many ways and with different fluorine content. In nature, a mineral occurs with the composition $Al_{16}(F,OH)_{48}\cdot 12-15H_2O$ (Rosenbergite), the Na- and Mg-free end-member of Ralstonite.[12] Cowley and Scott synthesized $AlF_x(OH)_{3-x}\cdot z(H_2O)$ with $x = 0.4-2.1$ by precipitation from solutions of aluminum fluorosulfate and treatment with ammonia,[13] whereas Roberson and Hem precipitated aluminum hydroxy fluorides from solutions containing aluminum, fluoride, sodium and perchlorate ions.[14] Grobelny obtained hydrated aluminum hydroxy fluorides by hydrothermal synthesis of aluminum fluoride solution and aluminum hydroxide.[15−17] Vanderheiden et al. prepared the basic aluminum fluorides by an electrolytic process in the system $AlCl_3\cdot 6H_2O$ and CaF_2 in water.[18] Another source of hydrated aluminum hydroxy fluoride is given by Plankey, Patterson, and Cronan.[19,20] They substituted water in reactions of $Al(H_2O)_6^{3+}$ and $Al(H_2O)_5OH^{2+}$ with F^- in aqueous solution. However, all of the products synthesized in one of these ways contain water and some of them even occur in multi phase mixtures.

Water free aluminum hydroxy fluorides can be obtained by direct fluorination of Al_2O_3 with hydrofluoric acid,[21] by thermal decomposition of $AlF_2(Ot\text{-}Bu)$[22] or $(NH_4)_3AlF_6\cdot zH_2O$[23] and by thermal dehydration of $AlF_3\cdot 3H_2O$.[23,24]

In 2003, we developed a direct sol−gel synthesis of metal fluorides using metal alkoxides and nonaqueous HF (eq 1).[25,26]

$$Al(OR)_3 + xHF \rightarrow AlF_x(OR)_{3-x} + xROH \quad (x = 0-3) \tag{1}$$

Metal fluorides prepared by this synthesis method are characterized by small particle size, a high surface area, and most notably, an exact adjustable fluorine content. To obtain the hydroxy fluorides, we have to hydrolyze the remaining Al-OR groups by water in a second step.[27] To combine these two steps, the fluorination and the hydrolysis of the alkoxide fluoride, we replaced the nonaqueous HF by hydrofluoric acid. With this new approach, the direct synthesis of aluminum hydroxy fluorides and aluminum fluorides in a one-pot sol−gel synthesis became possible.

2. Experimental Section

The aluminum hydroxy fluorides were prepared using Schlenk techniques under argon atmosphere because all of the precursor compounds are moisture-sensitive and the products all tend to adsorb water. Tetrahydrofurane (THF) was dried over Na and distilled prior to use. Aluminum isopropoxide and hydrofluoric acid (50 wt %) were purchased from Aldrich. The general procedure for the preparation of all aluminum (hydroxy)fluoride compounds is as follows: aluminum isopropoxide was dissolved in 100 mL dry THF to avoid an uncontrolled hydrolysation and hydrofluoric acid was slowly added in molar ratios Al:F = 1:n ($n = 1-6$, 0.16, 2.6) under stirring at room temperature. The resulting sol was stirred for 20 min followed by the removement of the solvent and formed isopropanole under reduced pressure. The final product was dried at 180 °C under vacuum.

Preparation of pseudoboehmite (AlOOH-xerogel):[28] Aluminum *sec*-butoxide was purchased from ABCR, nitric acid (65 wt %) was purchased from J. T. Baker. The boehmite-sol was prepared by adding aluminum *sec*-butoxide to water that was heated to a temperature of 90 °C and then stirring at high speed. The solution was kept at a temperature of 90 °C and, 45 min after addition of the alkoxide, 0.6 mol HNO_3 per mol alkoxide was added to peptize the sol particles. Following that, the solution was stirred another hour at a temperature of 90 °C. The solution was concentrated by evaporation and dried to constant weight at a temperature of 120 °C.

High-energy ball milling of pseudoboehmite and $AlF(OH)_2$ was performed in a commercial planetary mill "Pulverisette 7" (Fritsch, Germany) under the access of air applying milling times of 4 h. Each syalon vial was used with five syalon balls (m_{balls}, 14.8 g; m_{sample}, 1 g) and a rotational speed of 600 rpm (rotations per minute).

The thermal treatment of the samples was performed in a tube furnace in flowing air or argon (20 mL/min). To produce a moist atmosphere (moist air), we piped the flowing air through a water-filled bubble counter. The samples were heated (heating rate 20 K/min) to a temperature of 900 °C (dwell time 4 h).

For X-ray powder diffraction measurements, a Seiffert XRD 3003 TT equipment (Freiberg, Germany) with Cu K_α radiation was applied. Moisture-sensitive samples were prepared in a glovebox and covered with a special X-ray amorphous polystyrene foil. Phases were identified by comparison with the ICSD powder diffraction file.[29]

MAS NMR spectra were recorded at spinning speeds of 25 and 30 kHz and resonance frequencies of 376.4 MHz for ^{19}F and 104.6 MHz for ^{27}Al on a Bruker AVANCE 400 spectrometer equipped with a 2.5 mm MAS probe.

^{19}F MAS NMR ($I = 1/2$) spectra were recorded with a $\pi/2$ pulse duration of $p1 = 2$ μs, a spectrum width of 400 kHz, a recycling delay of 10 s, and an accumulation number of 64. Isotropic chemical shifts of ^{19}F are given with respect to the $CFCl_3$ standard. Background signals of ^{19}F could be completely suppressed with the application of a phase-cycled depth pulse sequence according to Cory and Ritchey.[30]

^{27}Al MAS NMR ($I = 5/2$) spectra were recorded with an excitation pulse duration of 1 μs. A 1 M aqueous solution of $AlCl_3$ was used as reference for the chemical shift of ^{27}Al. The recycle delay was chosen as 1 s and the accumulation number was 20 000.

Elemental analyses of the samples were performed with a LECO CHNS-932 combustion equipment (C, H, N). The fluoride contents

(12) Desborough, G. A.; Rostad, O. *Am. Mineral.* **1980**, *65*, 1057.
(13) Cowley, J. M.; Scott, T. R. *J. Am. Chem. Soc.* **1948**, *70*, 105.
(14) Roberson, C. E.; Hem, J. D. *Geochim. Cosmochim. Acta* **1968**, 32.
(15) Grobelny, M. *J. Fluorine Chem.* **1977**, *9*, 187.
(16) Grobelny, M. *J. Fluorine Chem.* **1977**, *9*, 441.
(17) Grobelny, M. *J. Fluorine Chem.* **1977**, *10*, 63.
(18) Vanderheiden, D. B.; Dumler, J. T.; Allen, D. R.; Allen, A. S. *Ind. Eng. Chem., Prod. Res. Develop.* **1968**, *7*, 220.
(19) Plankey, B. J.; Patterson, H. H. *Inorg. Chem.* **1989**, *28*, 4331.
(20) Plankey, B. J.; Patterson, H. H.; Cronan, C. S. *Environ. Sci. Technol.* **1986**, *20*, 160.
(21) Bulgakov, O. V.; Antipina, T. V. *Russ J. Phys. Chem. (Engl. Transl.)* **1967**, *41*, 1680.
(22) Johnson, R. L.; Siegel, B. *Nature (London, United Kingdom)* **1966**, *210*, 1256.
(23) Francke, L.; Durand, E.; Demourgues, A.; Vimont, A.; Daturi, M.; Tressaud, A. *J. Mater. Chem.* **2003**, *13*, 2330.
(24) Le Bail, A.; Jacoboni, C.; Leblanc, M.; De Pape, R.; Duroy, H.; Fourquet, J. L. *J. Solid State Chem.* **1988**, *77*, 96.
(25) Kemnitz, E.; Groβ, U.; Rüdiger, S.; Shekar, S. C. *Angew. Chem., Int. Ed.* **2003**, *42*, 4251.
(26) Rüdiger, S.; Groβ, U.; Kemnitz, E. *J. Fluorine Chem.* **2007**, *128*, 353.
(27) Prescott, H. A.; Li, Z.-J.; Kemnitz, E.; Deutsch, J.; Lieske, H. *J. Mater. Chem.* **2005**, *15*, 4616.
(28) Yoldas, B. E. *Am. Ceram. Soc., Bull.* **1975**, *54*, 289.
(29) JCPDS-ICDD - International Centre for Diffraction Data: mdit > PDF-2 Database (Sets 1−51 plus 70−89). PA 19073−3273 U.S.A., Release 2001. - PCPDFWIN Version 2.2.
(30) Cory, D. G.; Ritchey, W. M. *J. Magn. Reson.* **1988**, *80*, 128.

Table 1. Elemental Composition of Synthesized Samples[a]

n	Al (wt %)	F (wt %)	H (wt %)	O_{calcd}(wt %)	F/Al	O/Al	avg composition[b]
1	33.9	22.7	2.6	40.8	0.95	2.04	$AlF_{0.95}(OH)_{2.05}$
2	31.2	45.3	1.4	22.1	2.06	1.09	$AlF_{2.06}(OH)_{0.94}$
3	26.0	54.7	2.0	17.3	2.99	1.12	$AlF_3 \cdot 1.12H_2O$
4	n.d.	n.d.	1.8	n.d.	3	n.d.	$AlF_3 \cdot 0.9H_2O$
5	26.9	56.6	1.8	14.7	2.99	0.91	$AlF_3 \cdot 0.91H_2O$
6	n.d.	n.d.	1.6	n.d.	3	n.d.	$AlF_3 \cdot 0.8H_2O$
0.16	n.d.	n.d.	3.6	n.d.	0.16	n.d.	$AlF_{0.16}(OH)_{2.84}$
2.6	n.d.	n.d.	0.4	n.d.	2.6	n.d.	$AlF_{2.6}(OH)_{0.4}$

[a] *n* = equivalents of HF used per mole of Al(O*i*-Pr)$_3$; O_{calcd}, calculated oxygen content; F/Al, O/Al, molar ratios; n.d.: not determined. [b] In the text, the formulas were rounded using whole numbers for F and OH.

were determined with a fluoride sensitive electrode after conversion of the solids with Na_2CO_3/K_2CO_3 into a soluble form. The aluminum contents of the samples were determined by ICP OES (IRIS Intrepid HR DUO) after a microwave assisted (ETHOS plus) conversion with a H_3PO_4/HNO_3 mixture into a soluble form. The instrument was calibrated with standard solution.

Thermal analysis experiments were performed on a STA 409 C (Netzsch Gerätebau GmbH, Selb, Germany) equipped with a quadrupole mass spectrometer Balzers QMG 422. A

DTA-TG sample-holder system (Pt/PtRh10 thermocouple) was used. Measurements were performed in N_2-atmosphere.

The surface areas of the samples were determined using Ar absorption by means of a micromeritics ASAP 2020 instrument at 77 K. Before each measurement, the samples were degassed at 5 $\times 10^{-5}$ mbar and 150 °C for 12 h. The isotherms were processed by Brunauer−Emmett−Teller (BET) models.

High-resolution transmission electron microscopy (HRTEM) was conducted using a JEOL JEM-2200 FS with an acceleration voltage of 200 kV.

3. Results

Synthesis and Characterization. The synthesis of various metal fluorides via a sol−gel route using anhydrous HF in organic solvents was first developed in our group.[25,31] These reactions lead to X-ray amorphous metal alkoxide fluorides with very high specific surface areas.

The sol−gel synthesis of aluminum hydroxy fluorides ($AlF_x(OH)_{3-x}$, $AlF_3 \cdot zH_2O$) using aqueous HF solution leads to X-ray amorphous, and in the case of the aluminum hydroxy fluorides ($x \geq 1$), nonhydrated compounds with a stoichiometry extremely close to the chosen Al/F molar ratio. Table 1 shows the elemental composition of the synthesized samples.

The ^{27}Al MAS NMR spectra of $AlF(OH)_2$, $AlF_2(OH)$, and $AlF_3 \cdot 1.1H_2O$ (all formulas are rounded; the exact values are given in Table 1) are shown in Figure 1a−c. The spectrum of $AlF(OH)_2$ (Figure 1) shows at least four central signals with maxima of the chemical shift between 53 and −10 ppm. These peaks may represent AlF_xO_{4-x} species (53 ppm, $x = 0-4$),[32,33] AlF_xO_{5-x} species (26 ppm, $x = 0-5$)[32,33] and species with different average 6-fold Al coordination: AlF_xO_{6-x} with $x = 3-5$ (−4 pm and −10 ppm).[33,34] Because of the indistinguishability of $Al(OH)_x$-units from AlO_x-units in NMR, we use the notation AlF_xO_y to differentiate structural units from the sample composition. In the spectrum of $AlF_2(OH)$ (Figure 1, b) three signals between 50 ppm and −12 ppm can be resolved. The intensity of the peaks at 52 ppm and 25 ppm (AlF_xO_{4-x}- and AlF_xO_{5-x}-species, $x = 0-4$ and $x = 0-5$ respectively) is weaker than in the spectrum of $AlF(OH)_2$ because of the higher fluorine content in $AlF_2(OH)$. The maximum of the signal at −12 ppm is typical for species with a mean AlF_5O_1-coordination.[34,35] However, due to the asymmetric shape both in the high and low-field part of the ^{27}Al spectrum, other species with lower and higher fluorine proportion contribute. The spectrum of $AlF_3 \cdot 1.1H_2O$ (c) shows two signals in the ^{27}Al MAS NMR spectrum: a shoulder at 4 ppm (rests of AlO_6-species[32] or also AlF_1O_5-species[34]) and an asymmetric signal at −15 ppm typical for AlF_6-species. In all spectra, the maxima of the ^{27}Al signals shift to higher field with higher fluorine content and the presence of species with AlF_xO_{6-x} octahedra with $x \leq 5$ decreases.

A similar effect can be observed in the ^{19}F MAS NMR spectra of the samples (Figure 1d−f). The maximum of the average fluorine signal is shifted from −159 ppm ($AlF(OH)_2$, d) over −160 ppm ($AlF_2(OH)$, e) to −164 ppm ($AlF_3 \cdot 1.1H_2O$, f). The central ^{19}F signal of $AlF(OH)_2$ (Figure 1, d) is very broad and asymmetric. This asymmetry indicates the existence of different AlF_xO_{6-x} octahedra with $x \leq 4$[34,35] as the mean contribution, and this is supported by the results of the ^{27}Al MAS NMR measurement. $AlF_2(OH)$ gives a similar ^{19}F MAS NMR spectrum, but the line width of the central line is decreased and the peak is more symmetric. However, here too, the asymmetry indicates a distribution of different AlF_xO_{6-x} octahedra in the matrix with an increased number of species with high fluorine coordination ($x \geq 4$). The line width of the ^{19}F spectrum of $AlF_3 \cdot 1.1H_2O$ is the narrowest when comparing the ^{19}F spectra of Figure 1 (d-f), but even this line is not symmetric. The central line at −165 ppm is a clear argument for the existence of AlF_xO_{6-x} octahedra with an average value of $x \cong 5$ in the sample.[34,35] As expected, the line width decreases with higher fluorine content. In all three spectra two additional signals

(31) Rüdiger, S. K.; Groβ, U.; Feist, M.; Prescott, H. A.; Shekar, S. C.; Troyanov, S. I.; Kemnitz, E. *J. Mater. Chem.* **2005**, *15*, 588.
(32) Dressler, M.; Nofz, M.; Malz, F.; Pauli, J.; Jäger, C.; Reinsch, S.; Scholz, G. *J. Solid State Chem.* **2007**, *180*, 2409.
(33) Dambournet, D.; Demourgues, A.; Martineau, C.; Durand, E.; Majimel, J.; Vimont, A.; Leclerc, H.; Lavalley, J.-C.; Daturi, M.; Legein, C.; Buzaré, J.-Y.; Fayone, F.; Tressaud, A. *J. Mater. Chem.* **2008**, *18*, 2483–2492.
(34) König, R.; Scholz, G.; Pawlik, A.; Saeki, S.; Jäger, C.; van Rossum, B.; Oschkinat, H.; Kemnitz, E. *J. Phys. Chem. C* **2008**, in press.
(35) König, R.; Scholz, G.; Bertram, R.; Kemnitz, E. *J. Fluorine Chem.* **2008**, *129*, 598–606.

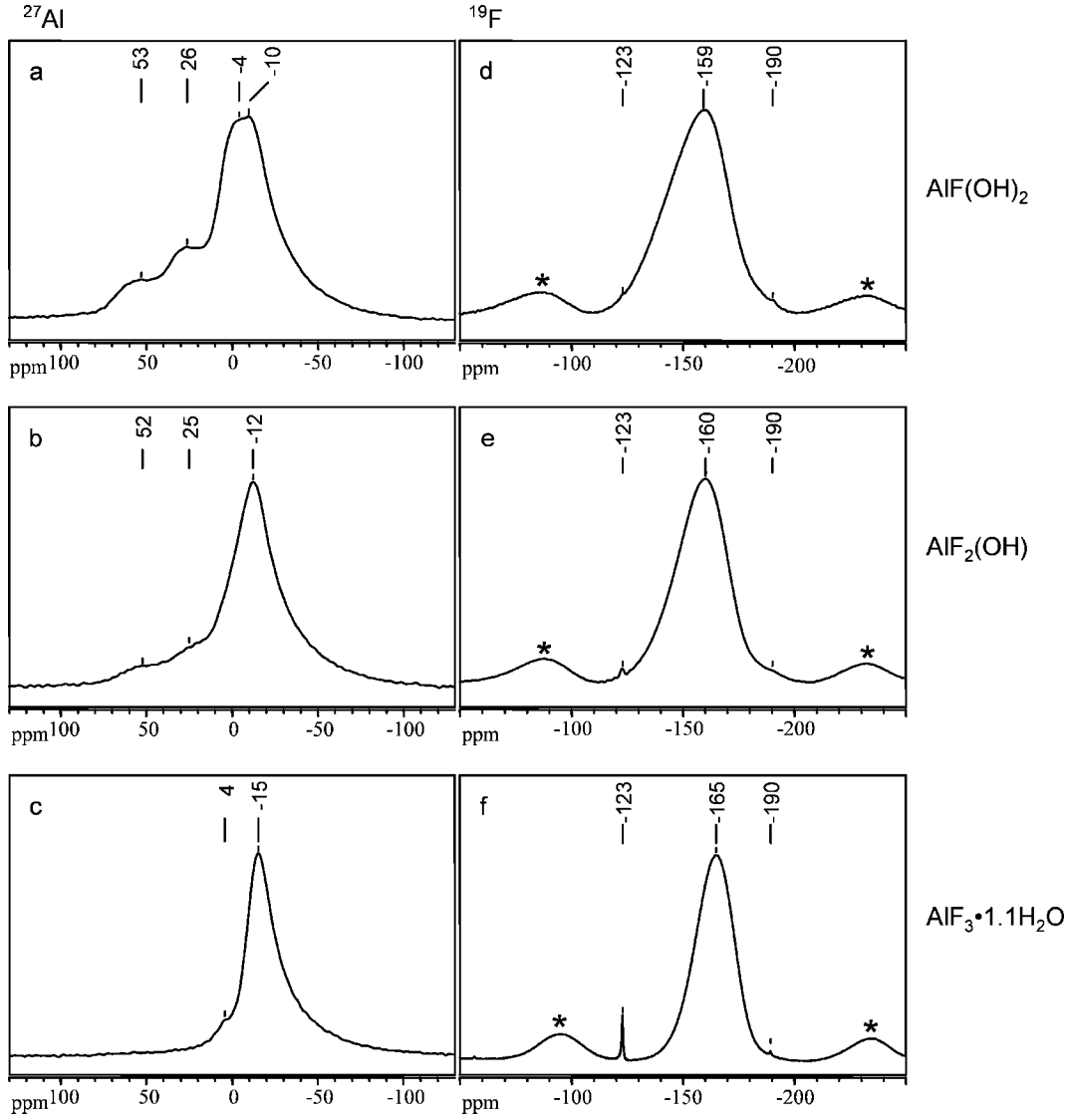

Figure 1. (a−c) ^{27}Al and (d−f) ^{19}F MAS NMR spectra (central lines) of the samples (a, d) $AlF(OH)_2$, (b, e) $AlF_2(OH)$, and (c, f) $AlF_3 \cdot 1.1H_2O$ after drying at 180 °C. All measurements were performed at a spinning speed of 25 kHz (*, spinning sidebands).

Table 2. BET Surface Area, Porosity Type, and Average Pore Diameter of Selected Samples

sample	surface area (m^2/g)	porosity type	avg pore diameter (Å)
$AlF(OH)_2$	495	mesoporous	30
$AlF_2(OH)$	502	mesoporous	90
$AlF_{2.6}(OH)_{0.4}$	215	mesoporous	134
$AlF_3 \cdot 1.1H_2O$	130	mesoporous	79
$AlF_3 \cdot 0.9H_2O$	3	mesoporous	57

at −123 ppm (possibly adsorbed HF)[36,37] and −190 ppm (terminal F sites) [38,39] can be observed.

The BET surface areas of the samples are shown in Table 2. The synthesis via a sol−gel route results, as expected, in high to very high surface areas.[25,31] Only in the case of $AlF_3 \cdot 0.9H_2O$ (molar ratio at synthesis, Al:F = 1:5) is the surface area extremely small.

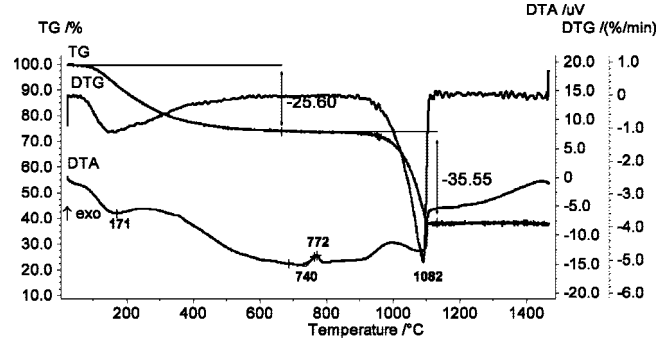

Figure 2. Thermoanalytic plot of $AlF(OH)_2$. Mass release of 25.60% (TG curve, first step) corresponds to the loss of water ($AlF(OH)_2 \rightarrow$ "AlFO" + H_2O).

Differential thermoanalysis (DTA) of $AlF(OH)_2$ (Figure 2) and $AlF_3 \cdot 1.1H_2O$ (Figure 3) are in agreement with the results of the elemental analysis. The mass losses of 25.6 and 19.9% correspond to the water release (calcd, 23.11 and 19.4%). The difference between the measured and calculated values is explainable by the generation of HF as a result of partial pyrohydrolysis of the samples caused by the released

(36) Delmotte, L.; Soulard, M.; Guth, F.; Seive, A.; Lopez, A.; Guth, J. L. *Zeolites* **1990**, *10*, 778.
(37) Guth, J. L.; Delmotte, L.; Soulard, M.; Brunard, N.; Joly, J. F.; Espinat, D. *Zeolites* **1992**, *12*, 929.
(38) Krahl, T.; Stö*β*er, R.; Kemnitz, E.; Scholz, G.; Feist, M.; Silly, G.; Buzare, J.-Y. *Inorg. Chem.* **2003**, *42*, 6474.
(39) Scholz, G.; Korup, O. *Solid State Sci.* **2006**, *8*, 678.

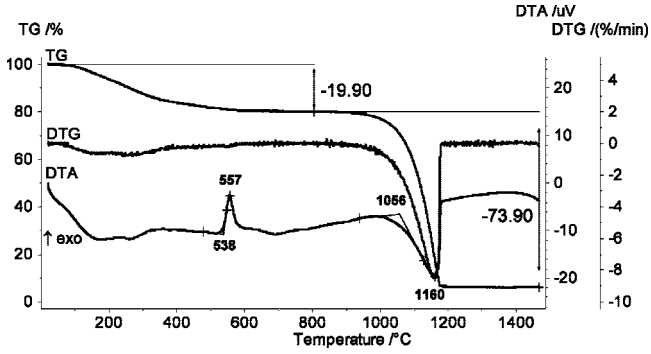

Figure 3. Thermoanalytic plot of $AlF_3 \cdot 1.1H_2O$. Mass release of 19.90% (TG curve, first step) corresponds to the loss of water ($AlF_3 \cdot 1.1H_2O \rightarrow AlF_3 + 1.1\ H_2O$).

water of the sample itself. The simultaneous H_2O and HF release occurs exactly in the temperature region described by Menz et al.[40]

Thermal Behavior. The gaseous atmosphere plays an important role in the thermal decomposition of aluminum hydroxy fluorides.[40,41] Menz et al. investigated the influence of partial pressure on the gaseous reaction products. Warf et al.[42] studied the reactions of various metal fluorides with water at high temperatures (pyrohydrolysis).

For this reason, we first studied the thermal behavior of the amorphous aluminum hydroxy fluorides in different gas atmospheres. Starting with $AlF_3 \cdot 1.1H_2O$. the X-ray diffractograms show different reaction products depending on the atmosphere (Figure 4). In argon only, pyrohydrolysis caused by the released water of the sample takes place. As a result of that, two phases (corundum and α-AlF_3) can be assigned with a high proportion of α-AlF_3. Thermal treatment of the sample in dry air also leads to the same phases. However, the content of α-Al_2O_3 seems to be much higher here. The usage of moist air leads to only one reaction product, α-Al_2O_3 (corundum). Here, all the fluoride obviously reacts completely with water and α-AlF_3 is no longer detectable by XRD. Figure 5 depicts the ^{27}Al and ^{19}F MAS NMR spectra of the same sample annealed in dry (c and e) and moist (d and f) air. After thermal treatment in dry air, the ^{27}Al MAS NMR spectrum of $AlF_3 \cdot 1.1H_2O$ (Figure 5c) shows two signals at 11 ppm (typical for α-Al_2O_3[43]) and -17 ppm (typical for α-AlF_3[39,44,45]). The corresponding ^{19}F MAS NMR spectrum (Figure 5e) shows only, in agreement with figure 5c, the typical signal of α-AlF_3 at -172 ppm. Spectra measured after annealing in moist air confirm the results of XRD measurements. Again, a signal at 12 ppm in the ^{27}Al MAS NMR spectrum (Figure 5d) indicates the existence of AlO_6 octahedra at the typical corundum position. A small signal at 60 ppm is due to rests of AlO_4 species in the matrix, belonging to a transition aluminum oxide[32] (not visible in XRD pattern (Figure 4)). The ^{19}F MAS NMR spectrum (Figure 5f) of the sample gives evidence for the high degree of pyrohydrolysis by the absence of a significant fluorine signal. Although the ^{19}F spectrum was recorded with the same number of accumulations (64), only weak signals in the range of -108 to -159 ppm with a worse signal-to-noise ratio were detected. They represent residual AlF_xO_{6-x} octahedra ($x \leq 4$) in the matrix.[34,35]

Comparable results were obtained after the thermal treatment of $AlF(OH)_2$ using these three atmospheres (Figure 6). After being annealed in an argon atmosphere, α-AlF_3 is observable together with traces of κ-Al_2O_3. In the case of thermal treatment in air (dry as well as moist air), oxidic phases (κ-Al_2O_3 and α- Al_2O_3) were detectable in XRD but the content of corundum is poor. The ^{27}Al MAS NMR spectrum of the sample annealed in dry air (Figure 5a) displays essentially three main central lines. Two of them belong to κ-Al_2O_3 (63 ppm and 11 ppm)[32] and α-Al_2O_3 (11 ppm), but the signal at -15 ppm indicates α-AlF_3 present in the matrix. In the ^{19}F MAS NMR spectrum (not shown here) the only peak at -173 ppm evidences the existence of α-AlF_3. In the ^{27}Al MAS NMR spectrum of the sample annealed in moist air (Figure 5b), only two signals at 63 ppm (κ-Al_2O_3) and 10 ppm (κ-Al_2O_3 and α-Al_2O_3) are observable. The low content of corundum is surprising because of the high surface area of this sample (495 m^2/g, see Table 2). It is well-known that a small particle size, very often connected with a high surface area, leads to a reduced phase transition temperature.[3,46,47] On the other hand, $AlF_3 \cdot 1.1H_2O$ with a surface area of "only" 130 m^2/g leads to corundum after thermal treatment at 900 °C in moist air. Since high-energy ball milling is a standard method to reduce the particle size,[43,48] $AlF(OH)_2$ was also milled for 4 h. After annealing the milled $AlF(OH)_2$ sample at 900 °C in moist air, the sample exclusively contained corundum (Figure 7).

Obviously, not only the fluorine content has an influence on the temperature of phase transition but also the particle size and the defect concentration introduced by mechanical activation. To verify this assumption, a pseudoboehmite (AlOOH-xerogel) was synthesized via the sol−gel route free of fluorine. Typical surface areas of pseudoboehmites lay between 160 and 220 m^2/g,[49] and hence, in between the surface areas of $AlF_3 \cdot 1.1H_2O$ and $AlF(OH)_2$. In Figure 8, the XRD patterns of the unmilled and the 4 h milled pseudoboehmite samples are shown. The quantity of reactive centers of the unmilled sample is insufficient to produce corundum after annealing. However, as observed for the milled $AlF(OH)_2$ sample, the milled pseudoboehmite also leads only to a proportional corundum phase containing residues of detectable transition aluminas after thermal treatment. The absence of fluorine seems to avoid the complete phase transition to corundum in this case. For

(40) Menz, D.; Mensing, C.; Hönle, W.; von Schnering, H. G. *Z. anorg. allg. Chem.* **1992**, *611*, 107.
(41) Kuznetsov, S. V.; Osiko, V. V.; Tkatchenko, E. A.; Fedorov, P. P. *Russ. Chem. Rev.* **2006**, *75*, 1065.
(42) Warf, J. C.; Cline, W. D.; Tevebaugh, R. D. *Anal. Chem.* **1954**, *26*, 342.
(43) Scholz, G.; Stö*β*er, R.; Klein, J.; Silly, G.; Buzaré, J. Y.; Laligant, Y.; Ziemer, B. *J. Phys.: Condens. Matter* **2002**, *14*, 2101.
(44) Dambournet, D.; Demourgues, A.; Martineau, C.; Pechev, S.; Lhoste, J.; Majimel, J.; Vimont, A.; Lavalley, J.-C.; Legein, C.; Buzaré, J.-Y.; Fayon, F.; Tressaud, A. *Chem. Mater.* **2008**, *20*, 1459.
(45) Silly, G.; Legein, C.; Buzaré, J. Y.; Calvayrac, F. *Solid State Nucl. Magn. Reson.* **2004**, *25*, 241.
(46) Gaffet, E.; Bernard, F.; Niepce, J.-C.; Charlot, F.; Gras, C.; Le Caër, G.; Guichard, J.-L.; Delcroix, P.; Mocellin, A.; Tillement, O. *J. Mater. Chem.* **1999**, *9*, 305.
(47) MacKenzie, K. J. D.; Temuujin, J.; Smith, M. E.; Angerer, P.; Kameshima, Y. *Thermochim. Acta* **2000**, *359*, 87.
(48) Fernández-Bertrán, J. F. *Pure Appl. Chem.* **1999**, *71*, 581.

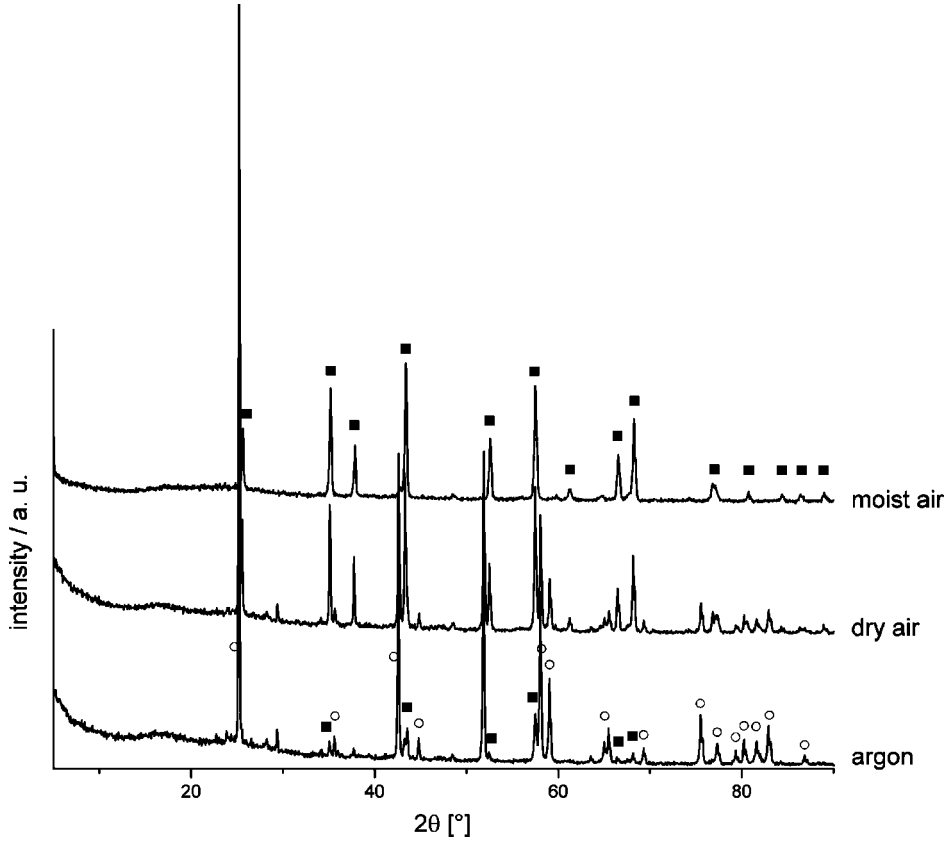

Figure 4. X-ray powder diffractograms of $AlF_3 \cdot 1.1H_2O$ after thermal treatment (4 h at 900 °C, 20 K/min) in different atmospheres. (■, reflections of α-Al_2O_3; ○, reflections of α-AlF_3).

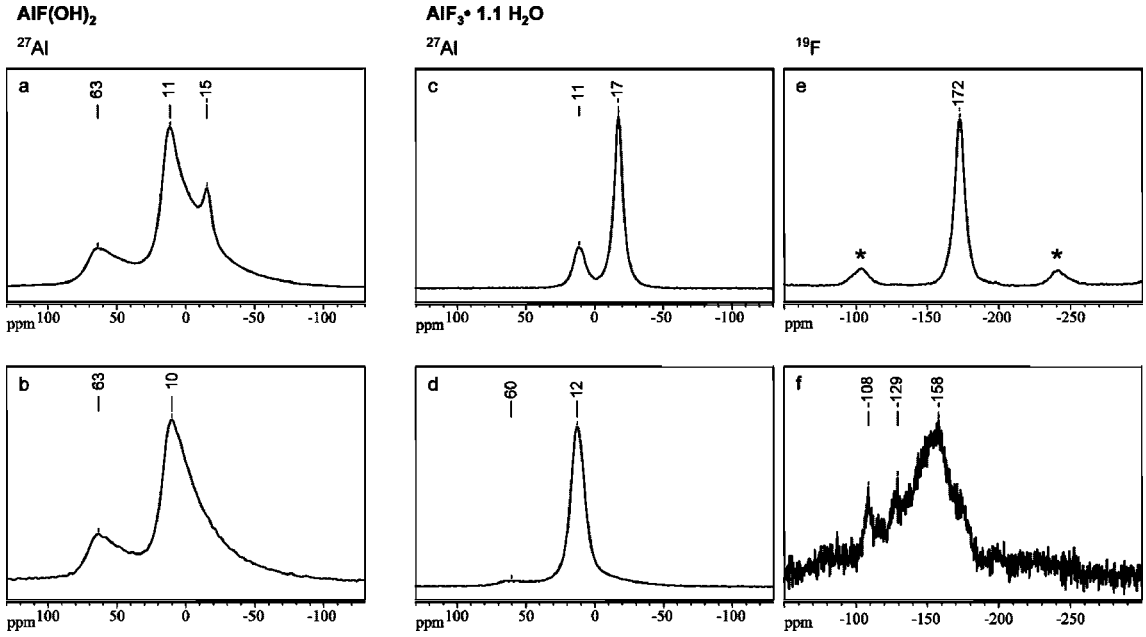

Figure 5. (a−d) ^{27}Al and (e, f) ^{19}F MAS NMR spectra (central lines) of (a, b) $AlF(OH)_2$ and (c−f) $AlF_3 \cdot 1.1H_2O$ after thermal treatment (4 h at 900 °C, 20 K/min) in dry (a, c, e) and moist (b, d, f,) air. All measurements were performed at a spinning speed of 25 kHz (*, spinning sidebands).

comparative purposes, in Figure 9, the XRD pattern of α-AlF_3, annealed under the same conditions (900 °C, moist air), are shown. This well-crystalline compound has a small surface area (~10 m^2/g) and a high fluorine content in contrast to pseudoboehmite. As expected, there are two phases after thermal treatment in moist air, α-AlF_3 and a corundum phase.

To investigate a larger variety of compositions between the fluorine free AlOOH-xerogel and α-AlF_3, several aluminum hydroxy fluorides with variable fluorine content were synthesized. All samples were annealed in moist air so that pyrohydrolysis became possible. In Figure 10 the annealed pseudoboehmite (Figure 10a) only shows reflections of transition oxides.[50,51] The XRD patterns of $AlF_{0.2}(OH)_{2.8}$

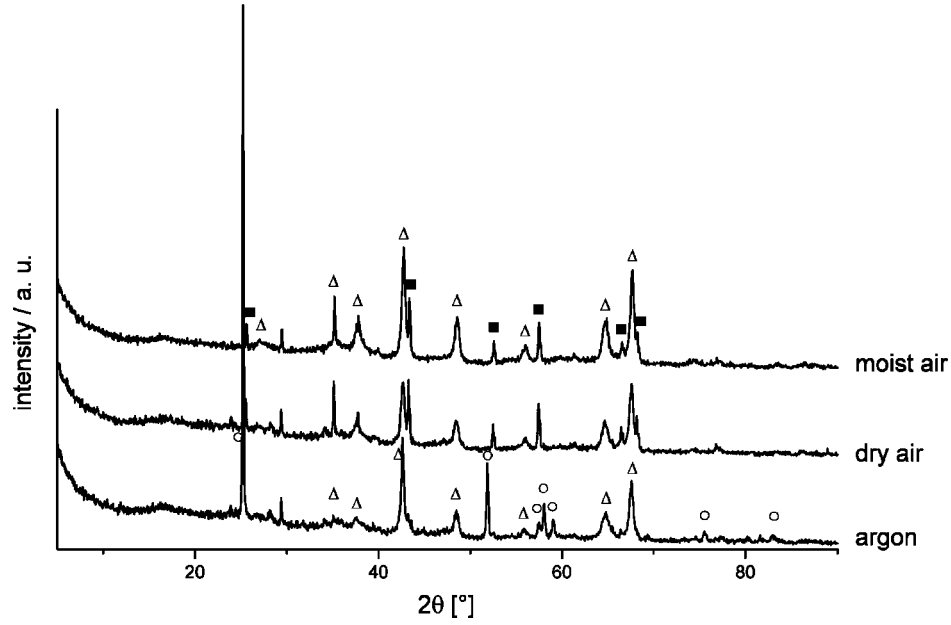

Figure 6. X-ray powder diffractograms of $AlF(OH)_2$ after thermal treatment (4 h at 900 °C, 20 K/min) in different atmospheres (Δ, reflections of κ-Al_2O_3; ○, reflections of α-AlF_3; ■, reflections of α- Al_2O_3).

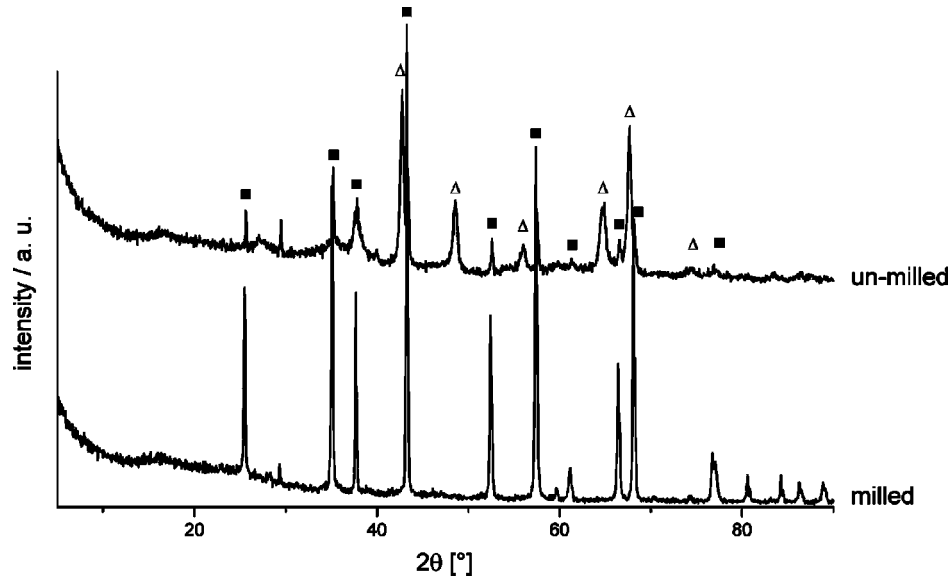

Figure 7. X-ray powder diffractograms of 4 h milled and unmilled $AlF(OH)_2$ after thermal treatment (4 h at 900 °C, 20 K/min) in moist air (Δ, reflections of κ-Al_2O_3; ■, reflections of α-Al_2O_3).

(molar ratio at synthesis: Al:F = 6:1) (Figure 10b), $AlF(OH)_2$ (molar ratio at synthesis: Al:F = 1:1) (Figure 10c), AlF_2-(OH) (molar ratio at synthesis: Al:F = 1:2) (Figure 10d) and $AlF_{2.6}(OH)_{0.4}$ (molar ratio at synthesis, Al:F = 1:2.6) (Figure 10e) recorded after thermal treatment are very similar. All samples consist of two phases: a major κ-Al_2O_3 phase and minor corundum phase. Only the content of corundum is slightly different. An abrupt change happens between $AlF_{2.6}(OH)_{0.4}$ (Figure 10e) and $AlF_3 \cdot 1.1H_2O$ (molar ratio at synthesis: Al:F = 1:3) (Figure 10f). The negligible change of the fluorine content leads to a rigorous change in the generated phase. Only corundum is detectable in XRD measurements. All samples with a fluorine content comparable with AlF_3, like $AlF_3 \cdot 1.1H_2O$ (molar ratio at synthesis, Al:F = 1:3, Figure 10f), $AlF_3 \cdot 0.9H_2O$ (molar ratio at synthesis, Al:F = 1:4, Figure 10g), $AlF_3 \cdot 0.9H_2O$ (molar ratio at synthesis: Al:F = 1:5, Figure 10h) and $AlF_3 \cdot 0.8H_2O$ (molar ratio at synthesis: Al:F = 1:6, Figure 10i) form corundum as the only oxidic phase. These experiments show the higher the fluorine content in these samples (Figure 10a−f), the better the generation of corundum after annealing. If the Al/F molar ratio at synthesis is higher than Al:F = 1:3 (Figure 10g−i), then a fluoridic phase is also detectable in XRD measurement (except $AlF_3 \cdot 0.9H_2O$ (molar ratio at synthesis, Al:F = 1:5, Figure 10h)).

4. Discussion

The sol−gel synthesis of aluminum hydroxy fluorides leads to highly disordered, nanoscaled, X-ray amorphous compounds. For this reason, the characterization of the samples was carried out using elemental analysis, MAS NMR experiments and DTA measurements. The elemental analysis

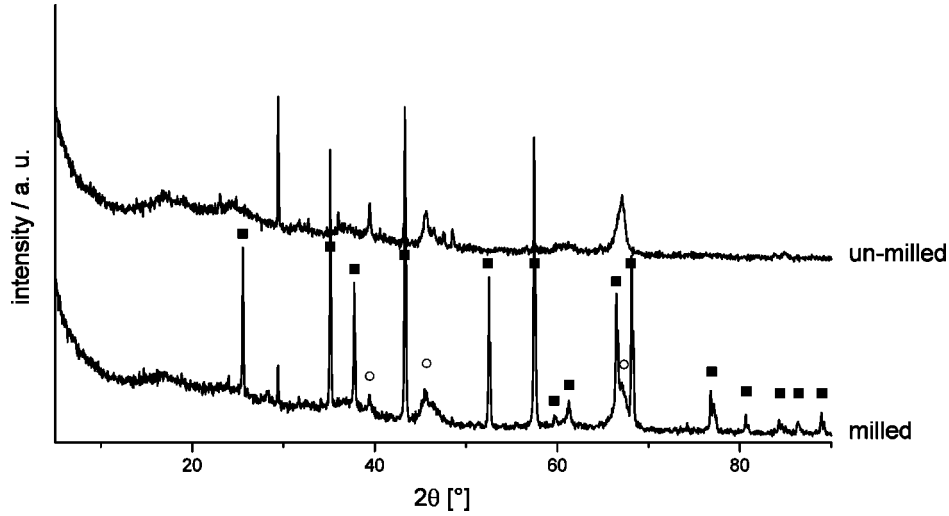

Figure 8. X-ray powder diffractograms of 4 h milled and unmilled pseudoboehmite (AlOOH-xerogel) after thermal treatment (4 h at 900 °C, 20 K/min) in moist air (■, reflections of α-Al_2O_3; ○, reflections of transition aluminas (ϵ, γ, δ, θ, and σ forms)).

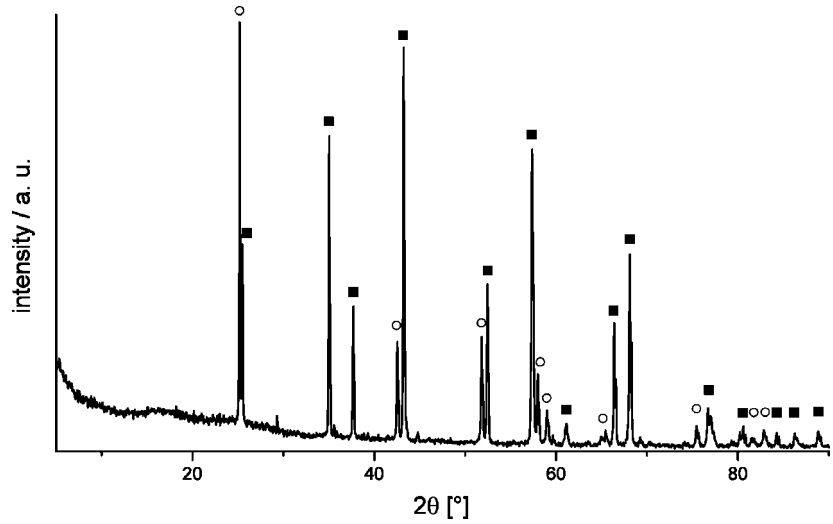

Figure 9. X-ray powder diffractogram of α-AlF_3 after thermal treatment (4 h at 900 °C, 20 K/min) in moist air (■, reflections of α-Al_2O_3; ○, reflections of α-AlF_3).

(Table 1) only shows the average composition of the samples. In general, two possibilities exist concerning a probable composition of such samples:

(i) two pure phases in coexistence, an aluminum fluoride and an aluminum hydroxide phase, or

(ii) a network of corner-shared $AlF_x(OH)_{6-x}$ species as described for chemically similar, well-defined crystalline samples with pyrochlore structure.[34,35]

The MAS NMR enables a local structural characterization of these samples in correlation to their elemental compositions. Exemplarily the samples with the mean composition $AlF(OH)_2$ and $AlF_3 \cdot 1.1H_2O$ will now be discussed.

Because of the results of ^{27}Al and ^{19}F MAS NMR measurements (a and d in Figure 1), possibility (i) can be excluded for $AlF(OH)_2$ (see refs 34, 35). The ^{27}Al spectrum explicitly shows the existence of different $AlF_x(OH)_{6-x}$ species beside AlF_xO_{5-x} and AlF_xO_{4-x} units. There were no direct indications for a coexistence of pure aluminum fluoride and aluminum hydroxide. The existence of 4- and 5-fold coordinated Al sites is an indicator of the structural manifold as a result of the sol−gel synthesis. The more intense signals at −4 and −10 ppm stand typically for AlF_3O_3 and AlF_4O_2 octahedra, as mentioned above, but again, the high degree of disorder of the structure makes a direct comparison of the chemical shift values between our samples and crystalline aluminum hydroxy fluorides difficult.[34,35,52] Distributions of bond lengths and angles of AlF_xO_{6-x} polyhedra lead to distributions of quadrupolar parameters, and therefore to a broadening of the signals and, in the case of ^{27}Al MAS NMR, to a shift of the signal maxima.[53,54] There have also been several investigations into the ^{19}F chemical shift of AlF_xO_{6-x} octahedra performed.[34,35,52,55] All these findings show that

(49) Yoldas, B. E. *J. Mater. Sci.* **1975**, *10*, 1856.
(50) Hill, M. R.; Bastow, T. J.; Celotto, S.; Hill, A. J. *Chem. Mater.* **2007**, *19*, 2877.
(51) Wefers, K.; Bell, G. M. *Tech. Pap. - Alcoa Res. Lab.* **1972**, *19*, 1.
(52) Chupas, P. J.; Corbin, D. R.; Rao, V. N. M.; Hanson, J. C.; Grey, C. P. *J. Phys. Chem. B* **2003**, *107*, 8327.
(53) Padro, D.; Howes, A. P.; Smith, M. E.; Dupree, R. *Solid State Nucl. Magn. Reson.* **2000**, *15*, 231.
(54) Weller, M. T.; Brenchley, M. E.; Apperley, D. C.; Davies, N. A. *Solid State Nucl. Magn. Reson.* **1994**, *3*, 103.
(55) Fischer, L.; Saeki, S.; Harlé, V.; Kasztelan, S.; d'Espinose de la Caillerie, J.-B. *Solid State Nucl. Magn. Reson.* **2000**, *16*, 85.

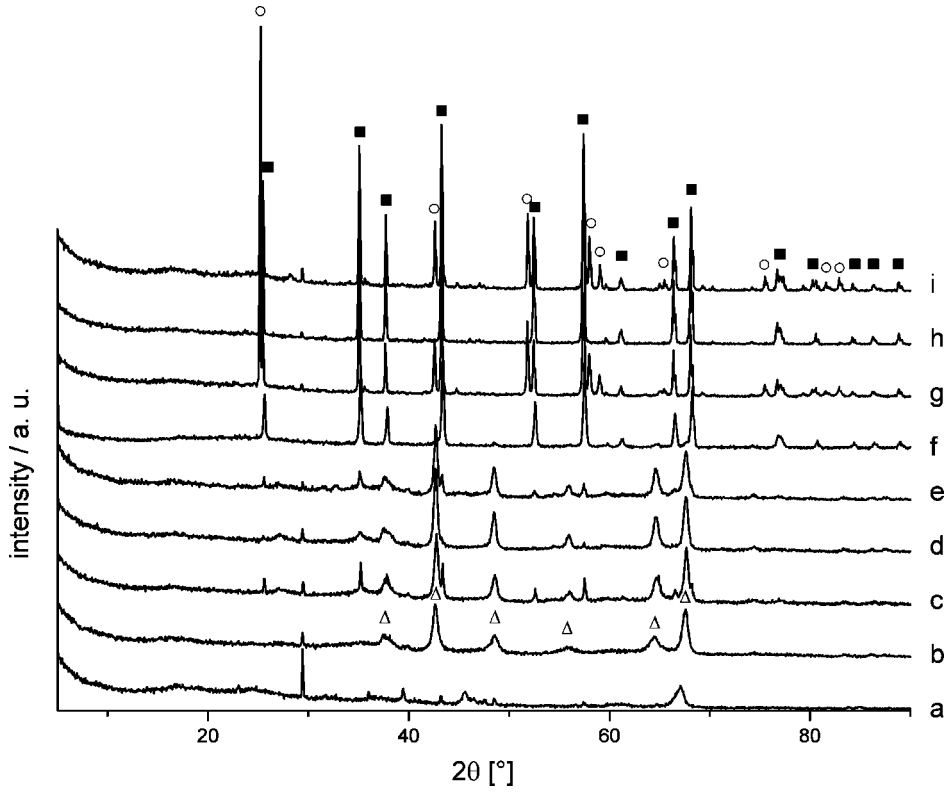

Figure 10. X-ray powder diffractograms of different aluminum hydroxy fluorides after thermal treatment (4 h at 900 °C, 20 K/min) in moist air. (a) Pseudoboehmite, for comparison; (b) $AlF_{0.2}(OH)_{2.8}$; (c) $AlF(OH)_2$; (d) $AlF_2(OH)$; (e) $AlF_{2.6}(OH)_{0.4}$; (f) $AlF_3 \cdot 1.1H_2O$ (Al:F = 1:3); (g) $AlF_3 \cdot 0.9H_2O$ (Al:F = 1:4); (h) $AlF_3 \cdot 0.9H_2O$ (Al:F = 1:5); (i) $AlF_3 \cdot 0.8H_2O$ (Al:F = 1:6)) Values in brackets: Al/F molar ratio at synthesis (■, reflections of α-Al_2O_3; Δ, reflections of*k*-Al_2O_3; ○, reflections of α-AlF_3).

the local environment of the F-atoms has a significant influence on the position of the ^{19}F MAS NMR signal. Chupas et al. created a ^{19}F chemical shift scale for AlF_xO_{6-x} octahedra in aluminum fluorophosphates.[52] König et al. developed chemical shift scales for ^{19}F of hydrated[35] and nonhydrated crystalline aluminum hydroxy fluorides.[34] Only the scale of the nonhydrated aluminum hydroxy fluorides[34] is directly comparable, because of the different chemical environments of the AlF_xO_{6-x} octahedra present in aluminum fluorophosphates[52] and hydrated aluminum hydroxy fluorides.[35] A comparison of the ^{19}F MAS NMR spectra of $AlF(OH)_2$, $AlF_2(OH)$, and $AlF_3 \cdot 1.1H_2O$ (Figure 1d−f), prepared in the present study continues the trend of the mean chemical shift value given in ref 35. The higher the fluorine content of the sample, the more the ^{19}F central signal experiences a high-field shift. On the basis of the scale developed by König et al. for crystalline nonhydrated aluminum hydroxy fluorides,[34] and bearing in mind the asymmetric shape of the ^{19}F signals especially in the low-field part (Figure 1d), there are indications for the existence of AlF_2O_4 octahedra (approximately −145 ppm), AlF_3O_3 octahedra (approximately −153 ppm), and AlF_4O_2 octahedra (approximately −159 ppm) in $AlF(OH)_2$. The very broad fluorine signal (Figure 1d) may also cover a certain proportion of higher fluorinated species like AlF_5O or AlF_6.

In the case of $AlF_3 \cdot 1.1H_2O$, the ^{27}Al and ^{19}F MAS NMR data (c and f in Figure 1) also exclude the possibility (i) of sample composition, i.e., the coexistence of aluminum fluoride and aluminum hydroxide. The ^{27}Al spectrum shows two signals, a shoulder at 4 ppm (typical AlO_6 species[32] or AlF_1O_5 species[34]) and an asymmetric peak at −15 ppm, a typical value for AlF_6 species.[34] In comparison to $AlF(OH)_2$, the maximum of the ^{19}F signal of $AlF_3 \cdot 1.1H_2O$ is, following the trend, shifted to higher field because of the higher fluorine content.[34,35,52] Again, the asymmetry of the spectrum is due to the superimposition of different signals belonging to AlF_xO_{6-x} octahedra with $x \geq 4$. Altogether the ^{19}F signal of $AlF_3 \cdot 1.1H_2O$ is narrower than the signals of $AlF(OH)_2$ and $AlF_2(OH)$ because of the lower content of AlF_xO_{6-x} octahedra with $x < 4$. Taking into account the information of both the ^{27}Al and ^{19}F spectra, the average Al coordination can be assigned between AlF_6 and AlF_5O, in agreement with the elemental analysis.

The thermoanalytic plots of $AlF(OH)_2$ and $AlF_3 \cdot 1.1H_2O$ support the results of elemental analysis and MAS NMR measurements. $AlF(OH)_2$ has a mass release (Figure 2, TG curve, first step) of 25.60%, which corresponds surprisingly well to the theoretical value of the mass loss of water ($AlF(OH)_2 \rightarrow$ "AlFO" + H_2O; calcd value, 23.11%). A subject of further investigations is the second step of the thermoanalytic plot of $AlF(OH)_2$ (Figure 2, TG curve). The mass loss of the second step (mass release, 35.55%) could depict the decomposition of AlOF into corundum and AlF_3 (3 AlOF $\rightarrow Al_2O_3 + AlF_3$). In this case, the sublimation of aluminum fluoride (sublimation temperature, ∼1270 °C) would cause a theoretical mass loss of 35%. $AlF_3 \cdot 1.1H_2O$ has a first mass release (Figure 3, TG curve) of 19.90%, which corresponds to the loss of water ($AlF_3 \cdot 1.1H_2O \rightarrow AlF_3 + 1.1\ H_2O$; calcd value, 19.38%), whereas the mass loss of the second step (73.9%) depicts the sublimation of AlF_3.

Hydrolysis of AlF_3 and generation of aluminum oxide (6.2 wt %) takes place as well, because of water traces in the atmosphere.

The gas atmosphere at annealing has a distinct influence on the generated phases. Therefore annealing of $AlF_3 \cdot 1.1H_2O$ in dry air (Figure 4) leads to a mixture of α-AlF_3 and α-Al_2O_3. The higher intensities of the α-AlF_3 reflections in the sample treated in argon atmosphere could be caused by a better sublimation of α-AlF_3 in air. This matter could be explained by the higher specific heat capacity ($c_{p,(air)} \approx 1$ kJ kg^{-1} K^{-1}, $c_{p,(Ar)} \approx 0.5$ kJ kg^{-1} K^{-1}) and the higher thermal conductivity ($k_{(air)} = 0.025$ W m^{-1} K^{-1}, $k_{(Ar)} = 0.017$ W m^{-1} K^{-1}) of air in comparison to argon. Also, the creation of vapor phase complexes[56,57] that contain oxygen and act as sublimation accelerator[58] is a possibility. The X-ray powder diffractograms of $AlF(OH)_2$ (Figure 6) show analogous effects. Again, the reflections of α-AlF_3 are more intensive after annealing $AlF(OH)_2$ in argon instead of dry air.

If the atmosphere is enriched with moisture, only aluminum oxides will be generated because of the pyrohydrolysis[42] (Figures 4 and 6). The pyrohydrolysis can be described by the general formula *:

$$\text{Al–F} + H_2O \longrightarrow \text{Al–OH} + HF \qquad (2)$$

In contrast to the aluminum hydroxy fluorides, the pyrohydrolysis of aluminum fluorides leads to a higher degree of structural disturbance because of the fact that nearly every Al—F bond in the compound must be broken whereas the Al—O bonds in the aluminum hydroxy fluorides were more stable against H_2O. This leads to an almost complete formation of corundum at low temperatures, as depicted in the MAS NMR spectra of $AlF_3 \cdot 1.1H_2O$ (d and f in Figure 5). Contrary to the annealing of $AlF_3 \cdot 1.1H_2O$ in dry air, where the ^{27}Al MAS NMR spectrum (Figure 5c) shows corundum (11 ppm) and α-AlF_3 (−17 ppm), the ^{27}Al spectrum of $AlF_3 \cdot 1.1H_2O$ annealed in moist air (Figure 5d) only shows a signal at 13 ppm (corundum) and a shoulder at 60 ppm (κ-Al_2O_3). Especially the comparison of the ^{19}F MAS NMR spectra of $AlF_3 \cdot 1.1H_2O$ annealed in dry (Figure 5e) and moist air (Figure 5f) displays the difference caused by the pyrohydrolysis. In the spectrum of $AlF_3 \cdot 1.1H_2O$ annealed in dry air, there is a signal at −173 ppm (typical value of α-AlF_3), whereas in the spectrum of $AlF_3 \cdot 1.1H_2O$ annealed in moist air nearly no fluoride is detectable (small signal-to-noise ratio). These results were confirmed by the XRD measurements of the sample (Figure 4).

The presence of moisture in the gas atmosphere also has a great influence on the thermal behavior of $AlF(OH)_2$ although the X-ray powder diffractograms of the samples annealed in dry and moist air were very similar (Figure 6). This influence can only be observed here by solid-state NMR. Both diffractograms show the typical reflections of a mixture of κ-Al_2O_3 and α-Al_2O_3. The existence of κ-Al_2O_3 is explainable by the presence of Al—O bonds, which will not be attacked by the pyrohydrolysis, and for that reason, there is a reduced disturbance of the structure of the sample. In both diffractograms, there were no hints of fluoridic phases, but the comparison of the ^{27}Al spectra of $AlF(OH)_2$ after thermal treatment shows a signal of α-AlF_3 (−16 ppm) beside signals of κ-Al_2O_3 (64 and 11 ppm) and α-Al_2O_3 (11 ppm) in the sample annealed in dry air (Figure 5a). In comparison, the spectrum of $AlF(OH)_2$ annealed in moist air (Figure 5b) consists only of signals belonging to κ-Al_2O_3 (63 and 10 ppm) and α-Al_2O_3 (10 ppm). In this spectrum, there is no aluminum fluoride detectable.

As mentioned above, the ratio of aluminum fluoride to aluminum oxide after thermal treatment in dry air depends directly on the amount of water released by the sample. This is visualized by the comparison of the intensities of the peaks in the ^{27}Al spectra of $AlF(OH)_2$ and $AlF_3 \cdot 1.1H_2O$ (a and c in Figure 5) at the values −17 ppm (α-AlF_3) and 11 ppm (corundum).

Another important condition for the formation of aluminum oxides is a high surface area of the samples, which is obtained by the sol−gel route. With the increase in the surface area, the number of reactive centers increases, too. The structural distortion lowers the temperature of phase transition[3,59] and additionally allows an easy hydrolysis of the Al—F bonds at the reactive centers. In Figure 8, the effect of milling of AlOOH-xerogel on the phase transition to corundum is shown. Both samples (milled and unmilled) were annealed at a temperature of 900 °C in moist air. The increased defect concentration obtained by milling leads to a corundum formation, whereas in the case of the unmilled sample "only" crystallization of transition aluminas is observable. The other effect of the presence of hydrolyzable Al—F-bonds is shown in Figure 7. In contrast to the unmilled $AlF(OH)_2$, the thermal treatment of $AlF(OH)_2$ in moist air after milling leads to the exclusive formation of corundum.

The overview of the X-ray powder diffractograms of all synthesized samples (Figure 10) shows the dependence of the habit of the oxidic phase after annealing in moist air on the fluoride content of the sample. As a result of the use of moist air, the amount of water stored in the sample in form of OH groups is irrelevant for a complete pyrohydrolysis. As long as the F:Al ratio of the samples is lower than 3:1 (Figure 10b−e), the generated aluminum oxide phase consists mainly of κ-Al_2O_3. However, all samples with an offered F:Al ratio higher than 3:1 (Figure 10f−i) form (proportional) corundum even at temperatures of 900 °C.

5. Conclusion

The present study provides a new synthetic route to aluminum hydroxy fluorides. The stoichiometry of the X-ray amorphous compounds obtained by the sol−gel synthesis with aqueous hydrofluoric acid is excellently adjustable as long the used F:Al ratio is less than 3:1. The samples have high surface areas and particle sizes in the nanoscale range

(56) Scholz, G.; Nieke, C.; Menz, D.; Kolditz, L. *J. Mol. Struct. (THEOCHEM)* **1991**, *231*, 95.
(57) Menz, D.; Scholz, G.; Becker, D.; Binnewies, M. *Z. Anorg. Allg. Chem.* **1994**, *620*, 1976.
(58) Ponikvar, M.; Liebman, J. F. *Struct. Chem.* **2006**, *17*, 75.
(59) Goodshaw, H. J.; Forrester, J. S.; Suaning, G. J.; Kisi, E. H. *J. Mater. Sci.* **2007**, *42*, 337.

(for HRTEM images of $AlF_3 \cdot 1.1H_2O$, see the Supporting Information). In spite of the synthesis in aqueous HF solution, the aluminum hydroxy fluorides are nonhydrated. It can be deduced that they are mainly composed of statistically distributed $AlF_x(OH)_{6-x}$ species as main components.

The influence of different gas atmospheres at annealing was investigated. It could be shown that the product composition after thermal treatment at 900 °C depends critically on the used atmospheres. Processes like AlF_3-sublimation or pyrohydrolysis can be enhanced or suppressed. The presence of moisture has the highest influence on the formed compounds after thermal treatment and leads to pure aluminum oxide phases without chemical impurities because of pyrohydrolysis.

Because of the disordered structure of the obtained aluminum hydroxy fluorides and the occurring pyrohydrolysis, the generation of pure, crystalline corundum succeeded even at 900 °C. The fluorine content of the samples favors pyrohydrolysis effects at annealing and early phase transition to corundum. A mechanical activation of the samples by milling supports the phase transition to corundum in addition.

Acknowledgment. The EU is acknowledged for support of part of this work through the 6th Framework Programme (FUNFLUOS, Contract NMP3-CT-2004-5005575). We further thank the DFG (Ke 489/22−2) for financial support. Dr. A. Zehl and U. Kätel are acknowledged for the elemental analysis, S. Bässler for the F-determination, Dr. M. Feist (all Humboldt-Universität zu Berlin, Institut für Chemie) for performing the thermoanalytical measurements. Dr. H. Kirmse (Humboldt-Universität zu Berlin, Institut für Physik) is acknowledged for the TEM measurements.

Supporting Information Available: High-resolution transmission electron microscopy (HRTEM) images of $AlF_3 \cdot 1.1H_2O$ (PDF). This material is available free of charge via the Internet at http://pubs.acs.org.

CM801236V